Dynamics of Calcium Clearance in Mouse Pancreatic β-Cells

Liangyi Chen,[1] Duk-Su Koh,[1,2] and Bertil Hille[1]

Pancreatic β-cells maintain glucose homeostasis by their regulated Ca^{2+}-dependent secretion of insulin. Several cellular mechanisms control intracellular Ca^{2+} levels, but their relative significance in mouse β-cells is not fully known. We used photometry to measure the dynamics of cytosolic Ca^{2+} ($[Ca^{2+}]_i$) clearance after brief, depolarization-induced Ca^{2+} entry. Treatment with thapsigargin or cyclopiazonic acid, inhibitors of the sarco-endoplasmic reticulum Ca^{2+}-ATPase (SERCA) pumps, nearly doubled the peak and slowed the decay of the depolarization-induced Ca^{2+} transients. The remaining thapsigargin-insensitive decay was slowed further by inhibition of the plasma membrane Ca^{2+}-ATPase (PMCA) and plasma membrane Na^+/Ca^{2+} exchanger (NCX) via alkalization of the bath solution, by adding lanthanum, or by substitution of Na^+ with Li^+. Mitochondrial Ca^{2+} uptake contributed little to clearance in thapsigargin-pretreated cells. Together, the SERCA, PMCA, and NCX transport mechanisms accounted for 89 to 97% of clearance in normal solutions. We developed a quantitative model for the dynamic role of removal mechanisms over a wide range of $[Ca^{2+}]_i$. According to our model, 50 to 64% of initial Ca^{2+} removal is via the SERCA pump, whereas the NCX contributes 21–30% of the extrusion at high $[Ca^{2+}]_i$, and the PMCA contributes 21–27% at low $[Ca^{2+}]_i$. *Diabetes* 52:1723–1731, 2003

The central importance of glucose homeostasis has drawn attention to the cell physiology of pancreatic β-cells. Insulin released from β-cells lowers blood glucose and facilitates glucose storage. Insufficient insulin secretion leads to diabetes. Several signal molecules modulate insulin secretion from β-cells (1), including cAMP (2), protein kinase A (3,4), protein kinase C (3,5), glutamate (6), malonyl-CoA (7,8), and insulin itself (9,10). However, cytosolic free Ca^{2+} ($[Ca^{2+}]_i$) is the dominant player in glucose-insulin-secretion coupling. Following a nutrient stimulus, β-cells depolarize, thereby causing the opening of voltage-gated Ca^{2+} channels. This leads to a brisk increase in calcium entry that initiates the exocytosis of insulin-containing granules. Hence, understanding intracellular Ca^{2+} dynamics is central for understanding insulin secretion.

As for other animal cells, four mechanisms remove Ca^{2+} from the cytosol of β-cells: the plasma membrane Na^+/Ca^{2+} exchanger (NCX), plasma membrane Ca^{2+}-ATPase (PMCA), sarco-endoplasmic reticulum Ca^{2+}-ATPase (SERCA) pumps, and the calcium uniporter of mitochondria (11–15). Together with cytosolic Ca^{2+} buffers, they determine the characteristics of $[Ca^{2+}]_i$ clearance. Many studies have examined these mechanisms, but it is not known how much each contributes to calcium removal in β-cells, which is the focus of our study.

We induced Ca^{2+} loads in mouse pancreatic β-cells by short membrane depolarizations while monitoring changes of the cytosolic free Ca^{2+}. Agents were applied to block each of the potential clearance mechanisms selectively. Our results show that the SERCA pumps dominate the clearance after depolarization.

RESEARCH DESIGN AND METHODS

Chemicals. Indo-1-AM, pluronic 147, and BCECF-AM were from Molecular Probes (Eugene, OR), and thapsigargin (TG) and cyclopiazonic acid (CPA) were from Calbiochem (La Jolla, CA). Culture medium, serum, and antibiotics were from Invitrogen (Carlsbad, CA), and all other chemicals from Sigma (St. Louis, MO).

Cell preparation. Animal care followed the University of Washington Animal Medicine guidelines. The pancreas was removed from male Balb/c mice (4–7 weeks old) killed with CO_2 (16), and islets of Langerhans were obtained by incubating small pancreatic pieces for 35 min in modified Hank's buffered solution, containing 5 mg/ml collagenase P (Boehringer, Germany), 1 mg/ml BSA, 20 mmol/l HEPES, and 10 mmol/l glucose. Single cells were dispersed by shaking islets in Ca^{2+}-free Hank's buffered solution containing 1 mmol/l EGTA, 5 mmol/l glucose, and 10 mg/ml BSA. Isolated cells plated on coverslips precoated with poly-ornithine were kept in a 37°C, 5% CO_2 incubator for 2–5 days in RPMI-1640 culture medium containing 10 mmol/l glucose, 10% FBS, 100 μg/ml streptomycin, and 100 IU/ml penicillin. Results were the same on culture days 2–5. Non–β-cells were excluded by selecting the larger cells (17). Frequent tests showed that these cells respond to high glucose with Ca^{2+} elevations and secretion (by amperometry).

Solutions. The control bath solution (called Na7.4) contained NaCl 130 mmol/l, KCl 2.5 mmol/l, $CaCl_2$ 2 mmol/l, $MgCl_2$ 1 mmol/l, HEPES 10 mmol/l, glucose 15 mmol/l, and diazoxide 250 μmol/l (pH 7.4 with NaOH). We included high glucose to mimic clearance under nutrient stimulus and diazoxide to minimize changes of the resting potential due to variations of cytoplasmic ATP. The experiments involved rapid changes (<500 ms) of solution by a fast local perfusion system controlled digitally. Except in Figs. 1, 5, and 7, depolarization and Ca^{2+} entry were evoked by 3-s applications of high K^+ solution containing KCl 70 mmol/l, NaCl 67 mmol/l, $CaCl_2$ 2 mmol/l, $MgCl_2$ 1 mmol/l, HEPES 10 mmol/l, glucose 15 mmol/l, and diazoxide 250 μmol/l (pH 7.4 with KOH). The KCl solution was followed by test solutions designed for selective study of specific Ca^{2+} clearance mechanisms. The test solutions were named by their principal cation and pH. Thus, to inhibit the NCX, we used Na^+-free solution with Li^+ replacing Na^+ (Li7.4). To slow the PMCA pump, we raised the pH 8.8 (Na8.8) (18) or added 200 μmol/l $LaCl_3$ (NaLa7.4)

From the [1]Department of Physiology & Biophysics, School of Medicine, University of Washington, Seattle, Washington; and the [2]Department of Physics, Pohang University of Science & Technology, Pohang, Korea.

Address correspondence and reprint requests to Bertil Hille, Department of Physiology & Biophysics, School of Medicine, University of Washington, Box 357290, Seattle, WA 98195-7290. E-mail: lychen@u.washington.edu

Received for publication 27 January 2003 and accepted in revised form 11 April 2003.

Additional information for this article can be found in an online appendix at http://diabetes.diabetesjournals.org.

$[Ca^{2+}]_i$, cytosolic free Ca^{2+}; CCCP, carbonyl cyanide *m*-chloro-phenylhydrazone; CPA, cyclopiazonic acid; ER, endoplasmic reticulum; NCX, Na^+/Ca^{2+} exchanger; PMCA, plasma membrane Ca^{2+}-ATPase; SERCA, sarco-endoplasmic reticulum Ca^{2+}-ATPase; TG, thapsigargin.

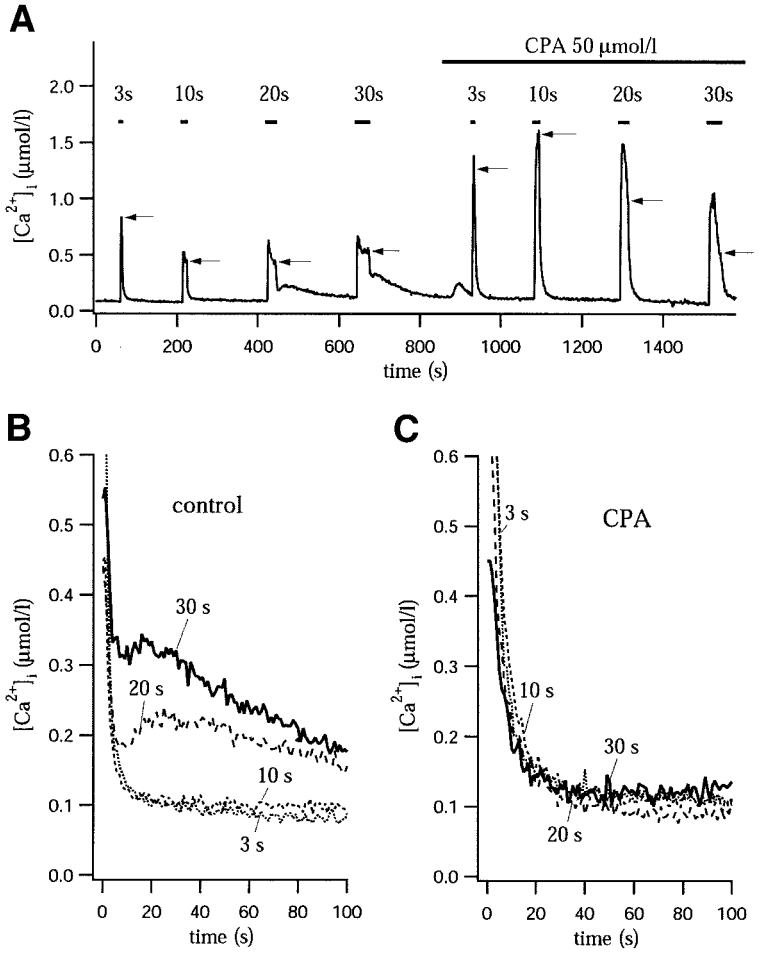

FIG. 1. Delayed Ca^{2+} release from the endoplasmic reticulum. *A*: Time course of $[Ca^{2+}]_i$ changes in a single pancreatic β-cell depolarized with 70 mmol/l K^+ perfusion (bars) for different durations as marked. Arrows show the Ca^{2+} level reached at the end of the depolarization. After the first four depolarizations, the cell was perfused with the SERCA pump blocker CPA (50 μmol/l; bar). The Na^+ solutions contained 15 mmol/l glucose plus 250 μmol/l diazoxide. *B*: Delayed Ca^{2+} release in aligned traces from the first four depolarizations in *A*. Zero time is the end of the depolarization, but in several traces, the initial points are clipped by the axes. *C*: Lack of delayed Ca^{2+} release in aligned traces from the second four depolarizations in *A* in CPA-containing solutions. This experiment is representative of a series of six similar experiments.

(19). Solutions Li8.8 and LiLa7.4 combined conditions to block two transporters. Other transport blockers were added to the Na7.4 bath solution. Flowing solutions were maintained at 35°C in all experiments with a heat exchanger.

Optical measurement of $[Ca^{2+}]_i$ and pH. Cytosolic Ca^{2+} was monitored with indo-1 (20). Briefly, cells were loaded with indo-1-AM (10 μmol/l) at room temperature for 20–25 min in a bath solution containing 4 mmol/l glucose. Sometimes, the loading solution also contained 1 μmol/l TG to block SERCA pumps. During $[Ca^{2+}]_i$ measurements, the dye was excited by 365 nm light, and two photomultipliers collected emission at 405 and 500 nm, respectively. The standard calibration parameters (21), R_{min} (0.406), R_{max} (4.8), and K* (2.688 μmol/l), were determined from cells equilibrated in KCl-based internal solutions containing ionomycin (10 μmol/l) and 20 mmol/l EGTA, 15 mmol/l $CaCl_2$, or 20 mmol/l EGTA with 15 mmol/l $CaCl_2$ (251 nmol/l free Ca^{2+}).

Cytosolic pH was monitored similarly in cells loaded with the ratiometric indicator BCECF-AM (1 μmol/l) for 20–25 min in standard bath solution (22). Excitation light at 440 and 490 nm was provided by a computer-controlled monochromator (T.I.L.L., Germany), and emitted light at 520 nm was collected by a photodiode. Calibration involved bathing cells in KCl-based "internal" solutions containing nigericin (10 μmol/l) at pH 5, 7, and 9 with 10 mmol/l MES, HEPES, or CHES buffers, respectively.

In the experiments of Fig. 5, Ca^{2+} dynamics were studied at 35°C in cells under whole-cell voltage clamp. The cells were held at –80 mV, and the pipette contained 100 μmol/l indo-1 dye and 75 mmol/l Cs_2SO_4, 15 mmol/l CsCl, 50 mmol/l HEPES, 6.5 mmol/l NaCl, 2.5 mmol/l sodium pyruvate, 2.5 mmol/l malate, 1 mmol/l NaH_2PO_4, 1 mmol/l $MgSO_4$, 5 mmol/l MgATP, and 0.3 mmol/l tris-GTP (pH 7.3 with CsOH). Calcium loading was induced in a bath medium containing 10 mmol/l Ca^{2+} and 10 mmol/l tetraethylammonium ion by stepping the membrane potential to 0 mV for only 300–400 ms. Potentials were corrected for a –10 mV junction potential.

Amperometric measurement of vesicular secretion. Cells were preincubated in culture medium supplemented with the oxidizable neurotransmitter serotonin (1.5–2 mmol/l) for 7–14 h (23). A carbon-fiber electrode (24) was connected to an EPC-9 patch clamp amplifier (HEKA, Lambrecht, Germany) and held at 600 mV. Serotonin coreleased from individual insulin-containing granules was detected by the electrode as spikes of oxidation current.

Calculations. Data were analyzed and modeled in Igor Pro (Wavemetrics, Lake Oswego, OR). Averaged results are given as means ± SE. Statistical significance was assessed using unpaired Student's *t* test. The rate equations of a kinetic model given later were integrated numerically by the Euler method (first-order integration) in time steps of 0.5 s (see also ONLINE APPENDIX).

RESULTS

Delayed release of Ca^{2+} from stores. The experiments measured the time course of $[Ca^{2+}]_i$ decay following depolarization-induced Ca^{2+} loads. Ideally, by selectively inhibiting specific clearance mechanisms, one could determine the contribution and rate laws of each mechanism. An important assumption of this approach is that the evoked delivery of Ca^{2+} to the cytoplasm stops as soon as the Ca^{2+}-loading depolarization is over. Past work on β-cells with slow perfusion and ≥30 s KCl depolarizations had shown that Ca^{2+} entry could be followed by a delayed release of Ca^{2+} from the endoplasmic reticulum (ER) that lasts >1 min (25,26). Therefore, our first experiments explored how to minimize this interfering phenomenon.

Figure 1*A* shows $[Ca^{2+}]_i$ measurements as the 70 mmol/l K^+ depolarizing solution is applied repeatedly to a single β-cell for times ranging from 3 to 30 s. The $[Ca^{2+}]_i$ rises steeply during each depolarizing stimulus and then falls as transporters clear it away from cytosol. The falling phases are aligned and superimposed on a faster time scale in Fig. 1*B* and *C*. Consider the first four test depolarizations in which none of the clearance mechanisms is inhibited: after

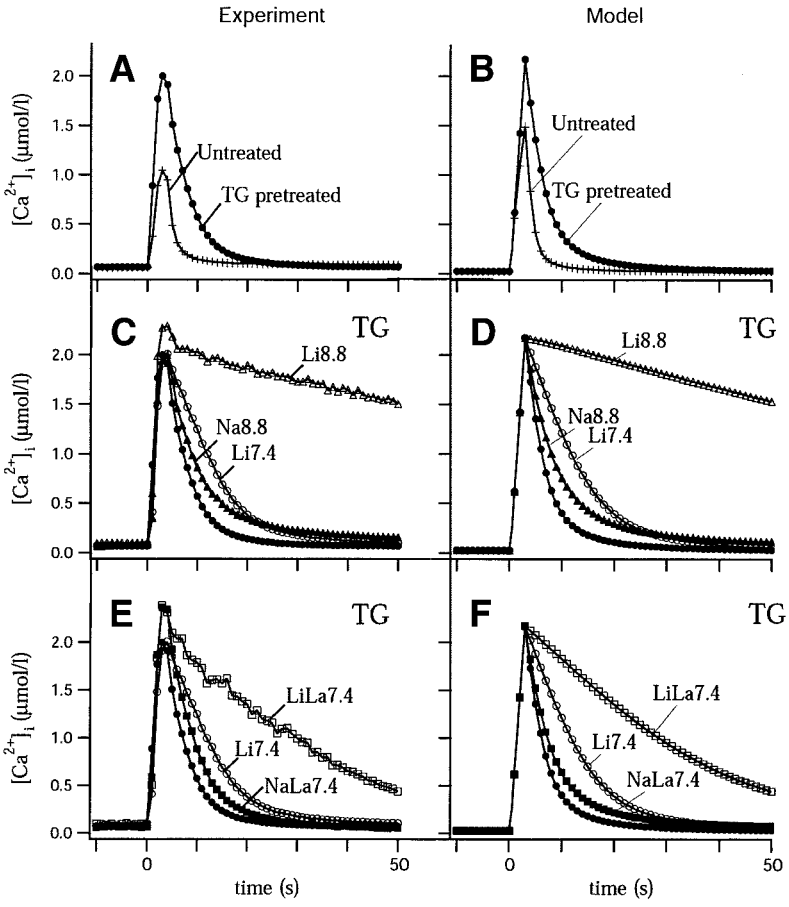

FIG. 2. Experimental and simulated Ca^{2+} recoveries after short depolarizations. *A* and *B*: Averaged and simulated clearances in 35 cells pretreated with 1 μmol/l TG (●) and 135 cells not pretreated with TG (+). *C* and *D*: TG-pretreated cells in control (●), Li7.4 (○), Na8.8 (▲), and Li8.8 (△) solutions. *E* and *F*: TG-pretreated cells in control (●), Li7.4 (○), NaLa7.4 (■) and LiLa7.4 (□) solutions. All experiments involve 3-s KCl depolarizations starting at time 0 s. The simulations are described in the text ("Model"), in the ONLINE APPENDIX, and in Fig. 6.

the 3- and 10-s depolarizations, the decay of $[Ca^{2+}]_i$ is monotonic, and $[Ca^{2+}]_i$ returns to its resting level with an exponential time constant <2 s. After the 20- and 30-s depolarizations, recovery is not monotonic and shows a hump indicative of a delayed Ca^{2+} release. However, the decay becomes monotonic in the second half of the experiment (Fig. 1*A* and *C*), where the SERCA pumps are inhibited with CPA. Evidently, the delayed Ca^{2+} release requires prior filling of the ER stores (25) and does not occur without a large Ca^{2+} load or when SERCA pumps are blocked. In all subsequent experiments, we prevented the delayed Ca^{2+} release by using short (3 s) exposures to the depolarizing solution and, often, by preincubating the cells with the irreversible SERCA pump inhibitor TG as well.

The experiments of Fig. 1 suggest that considerable Ca^{2+} removal occurs *during* longer depolarizing pulses. At the end of 10-, 20-, and 30-s depolarizations, $[Ca^{2+}]_i$ is *lower* (see arrows) than after a 3-s depolarization, because voltage-gated Ca^{2+} channels inactivate enough within a few seconds (27) that the entry rate during the pulse falls below the clearance rate. Thus, depolarizing for only 3 s allowed us to study clearance starting at a *higher* initial $[Ca^{2+}]_i$ level in a cell whose intracellular organelles did not already have a large Ca^{2+} load.

SERCA pumps dominate Ca^{2+} clearance. The contribution of SERCA pumps to Ca^{2+} clearance was assessed by comparing $[Ca^{2+}]_i$ decay before and after inhibition with CPA or TG. With 3-s depolarizations, these inhibitors increased the peak amplitude of the Ca^{2+} transients and slowed their subsequent decay (Figs. 1 and 2*A*). Thus, SERCA pumps are important in removing Ca^{2+} both during the 3 s of depolarization and in the subsequent recovery. Consider the averaged traces in Fig. 2*A*. Inhibition of SERCA pumps doubles the peak Ca^{2+} evoked by depolarization, from 1.06 ± 0.07 μmol/l (n = 35) in control cells to 2.05 ± 0.04 μmol/l (n = 130) in TG-pretreated cells.

Rates of Ca^{2+} increase during the depolarization and rates of Ca^{2+} decrease during the recovery are plotted as a function of $[Ca^{2+}]_i$ in Fig. 3*A*. These points are derived from the time derivatives of the averaged traces of Fig. 2*A*. TG pretreatment elevated the rate of rise of $[Ca^{2+}]_i$ during the depolarization from 0.41 to 0.85 $\mu mol \cdot l^{-1} \cdot s^{-1}$ at 0.48 μmol/l $[Ca^{2+}]_i$ and reduced the rate of decay during the recovery from ~0.32 to 0.1 $\mu mol \cdot l^{-1} \cdot s^{-1}$ at 0.48 μmol/l $[Ca^{2+}]_i$. Thus SERCA pumps remove about two-thirds of the Ca^{2+} load during the depolarization and recovery. The same conclusion is reached by fitting the falling phase of the Ca^{2+} transients with single exponential functions. Compared with control cells, TG pretreatment prolongs the recovery time constant τ, from 1.7 ± 0.1 to 4.6 ± 0.1 s, a 63% reduction of the rate of clearance (Fig. 3*B*).

As a further check that these results were not contaminated by excessive loading of the ER, we repeated the experiments on cells under whole-cell voltage clamp using brief (300–400 ms) step depolarizations and 100 μmol/l indo-1 inside. The bathing $[Ca^{2+}]_i$ was raised to 10 mmol/l to enhance the rate of entry during these shorter depolarizations. The clearance time constant (1.0 ± 0.1 s) (Fig. 3*B*) was slightly shorter than in intact cells, and the effect of TG was virtually the same as in intact cells (τ = 4.4 ± 0.3 s). The shorter time constant in whole-cell recording

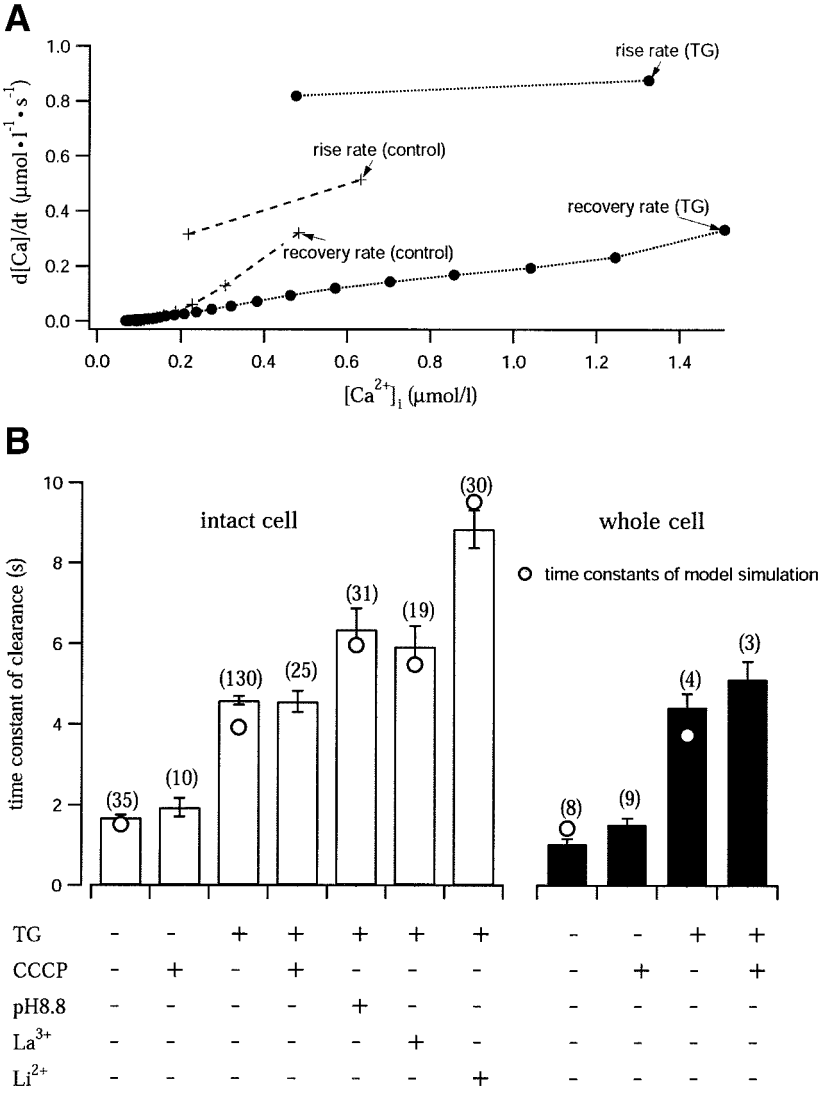

FIG. 3. Quantitative measures of Ca^{2+} entry and clearance. *A*: The absolute value of the rate of change of $[Ca^{2+}]_i$ in control (+) and TG-pretreated cells (●) during and after KCl depolarizations, plotted as function of $[Ca^{2+}]_i$. *B*: Summary of the recovery time constants in different solutions (number of cells in parentheses). Individual calcium recovery traces are fitted with single-exponential functions and the mean ± SE time constant is given here as a bar. Time constants from the model simulations in Fig. 2*B*, *D*, and *F* are shown as open symbols.

can be explained largely by the lower cellular indo-1 concentration under whole-cell recording (see below, "Relative contributions to Ca^{2+} clearance and a model").

Contributions of the NCX and PMCA in TG-pretreated cells. Subsequent experiments were done with cells pretreated with TG to block SERCA pumps, permitting better resolution of other slower clearance mechanisms. To stop forward operation of the NCX, we replaced all Na^+ with Li^+ (28). After a control KCl depolarization, cells were washed with control solution for 150 s, and after a second depolarization, they were exposed to the Li7.4 solution for 100 s. Aligning averaged traces to the start of the depolarization shows that the Li7.4 solution slows the initial rate of Ca^{2+} clearance (Fig. 2*C*, Li7.4). Turning off the NCX lengthens the recovery time constant from 4.6 ± 0.1 to 8.9 ± 0.5 s (Fig. 3*B*), a 48% reduction of clearance in these TG-pretreated cells. A blocker of reverse-mode (Ca^{2+} influx) operation of the NCX, KB-R7943 (5 μmol/l), did not affect Ca^{2+} clearance time course in TG-pretreated cells (data not shown).

Two approaches were used to block the PMCA. Because the PMCA exports one cytosolic Ca^{2+} in exchange for one or two extracellular protons, lowering the proton concentration in the bath slows pumping (18). We found that raising the pH in the bath solution to 8.8 (Na8.8) slowed especially the late phase of Ca^{2+} clearance (Fig. 2*C*). Because alkalization might alter Ca^{2+} clearance in other ways than blocking the PMCA, we also used another blocker, La^{3+}, at 0.2 mmol/l, a concentration reported to inhibit the PMCA but not the NCX (19). When La^{3+} was added to the bath solution (NaLa7.4), the initial kinetics of recovery (Fig. 2*E*) were similar to those observed in Na8.8 solution (Fig. 2*C*), but below 0.5 μmol/l Ca^{2+}, the NaLa7.4 trace returned more quickly to the basal level. The recovery time constants in Na8.8 and NaLa7.4 solutions were 6.4 ± 0.5 and 5.9 ± 0.5 s, respectively, in comparison to a control value of 4.6 ± 0.1 s in TG-pretreated cells (Fig. 3*B*), a 40 or 28% additional slowing of Ca^{2+} clearance rates. Modeling shown below suggests that the difference represents less blockade of the PMCA by 0.2 mmol/l La^{3+}. As reported by others (19), higher concentrations of La^{3+} seemed to inhibit both the NCX and the PMCA and were not explored further.

To test whether the SERCA, PMCA, and NCX mechanisms together account for most of the clearance from β-cells, we blocked all three of them simultaneously. The cells were pretreated with TG and then switched to a Na^+-free Li^+ solution either with high pH (Li8.8) or with

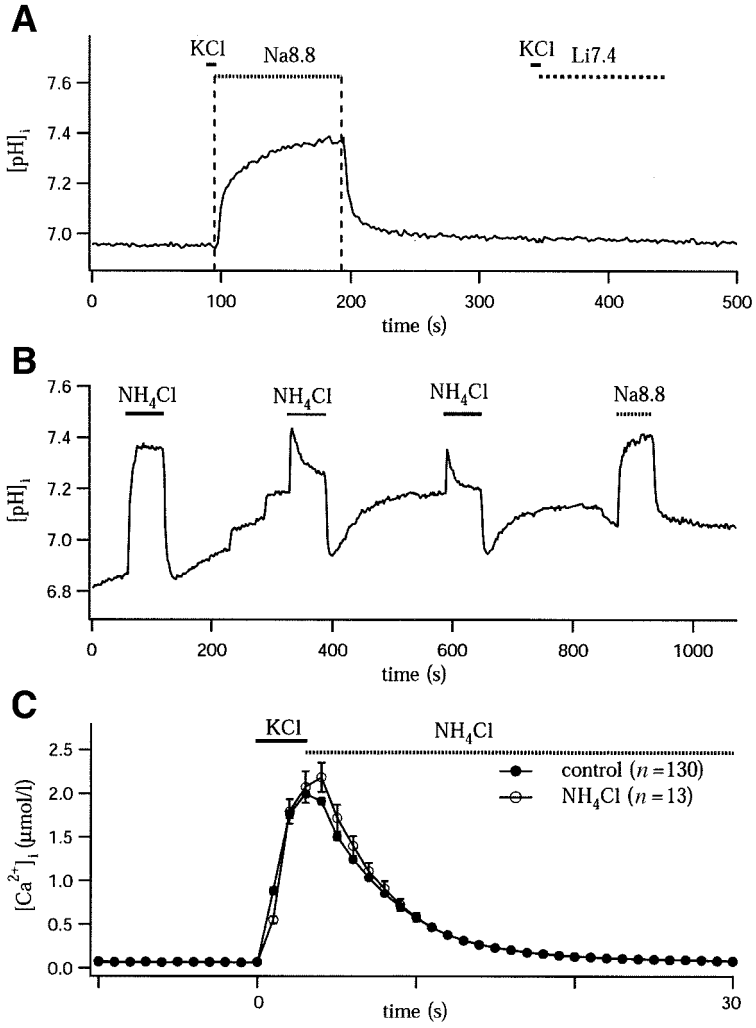

FIG. 4. Intracellular pH changes. *A*: Intracellular pH monitored in BCECF-loaded and TG-pretreated cells during treatments with KCl (70 mmol/l, 5 s), Na8.8, and Li7.4 solutions. *B*: Comparison of intracellular pH changes during perfusion with ammonium chloride (20 mmol/l) and Na8.8 solutions. *C*: Comparison of Ca^{2+} clearance in control solution (●, $n = 12$) and in NH_4Cl (○, $n = 12$).

0.2 mmol/l La^{3+} (LiLa7.4) immediately after depolarization by KCl. The Li8.8 solution slowed the recovery dynamics extremely (Fig. 2*C*), indicating that the three transport mechanisms account for almost all of the normal clearance. As expected, the LiLa7.4 solution slowed recovery also, but not as much (Fig. 2*E*).

A possible artifact of bath alkalization or sodium substitution is to increase *intracellular* pH and thereby alter other clearance mechanisms. We therefore measured cytosolic pH with the indicator BCECF. Indeed, switching to the alkaline extracellular solution (Na8.8) did increase intracellular pH of BCECF-loaded cells but only by about 0.45 ± 0.06 units, to pH 7.2 within 20 s ($n = 6$) (Fig. 4*A*). Replacement of Na^+ with Li^+ induced no pH changes. The following control experiments show that a 0.4-unit intracellular pH increase does not affect the PMCA or the NCX: we found that a bath solution containing 20 mmol/l NH_4Cl produces an intracellular pH increase similar to that of Na8.8 (Fig. 4*B*) (22), without altering Ca^{2+} clearance in TG-pretreated cells (Fig. 4*C*).

Lack of effects of mitochondria in TG-pretreated cells. Is there a role of mitochondria in Ca^{2+} clearance of TG-pretreated cells? Mitochondrial Ca^{2+} uptake is driven by the large mitochondrial membrane potential (negative inside), so the standard approach to stop Ca^{2+} uptake is to collapse the mitochondrial membrane potential with a protonophore like carbonyl cyanide *m*-chloro-phenylhydrazone (CCCP). A possible artifact is that cellular ATP is gradually depleted, so the PMCA and SERCA pumps might be slowed. As this could happen in intact β-cells despite the short time of our experiments, we did experiments on TG-pretreated cells under whole-cell voltage clamp with 5 mmol/l ATP in the pipette, as well as on intact cells. In either case, 50-s CCCP treatments did not change the exponential time constants of Ca^{2+} decay (Figs. 3*B* and 5*A*). For intact cells, the resting Ca^{2+} level was very slightly elevated with 2 μmol/l CCCP plus 2.5 μmol/l oligomycin, but the time constant (4.6 ± 0.3 s) was the same as in TG-pretreated control cells (4.6 ± 0.1 s), and for clamped cells, the time constant with 2 μmol/l CCCP was 5.1 ± 0.4 s, not significantly different from control (4.4 ± 0.3 s). Thus, we conclude that mitochondrial Ca^{2+} uptake is not a major contributor to the Ca^{2+} clearance we see after 0.3- to 3-s depolarizations. Nevertheless, a puzzling finding was that CCCP raised resting $[Ca^{2+}]_i$ and slowed clearance by 15% ($P = 0.16$, NS) in intact and 45% ($P = 0.006$) in clamped cells not pretreated with TG (Fig. 3*B*). This slowing could be a sign of local ATP depletion during CCCP treatment and might reflect some close interaction of mitochondria with the ER or a lack of specificity of the inhibitors, but we lack a clear explanation. The lack of effect of CCCP on TG-pretreated cells is not likely a block

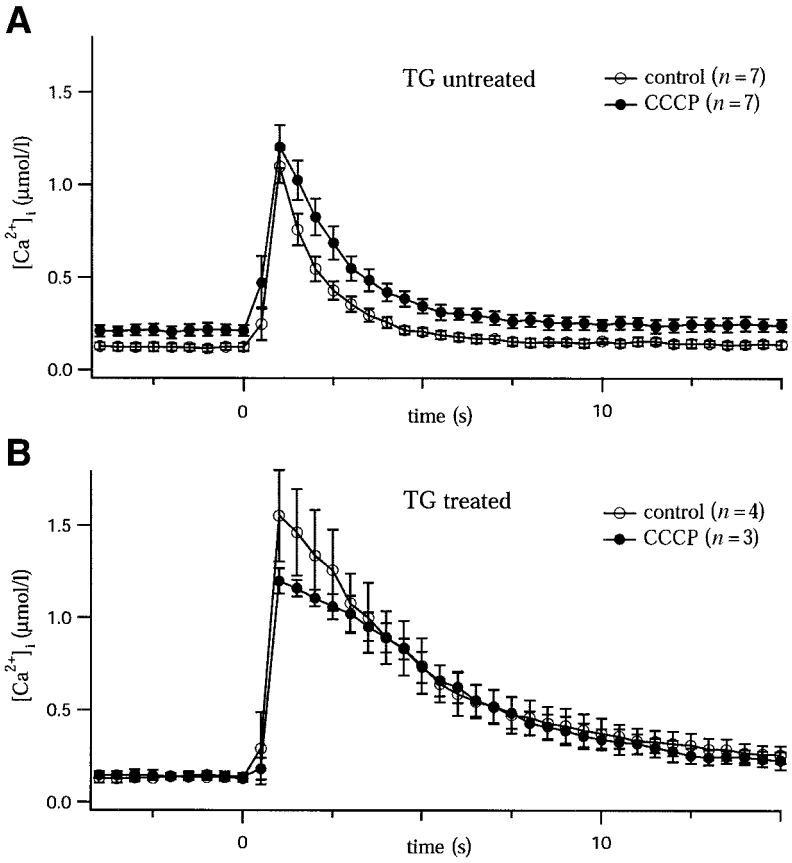

FIG. 5. Contribution of mitochondria to Ca^{2+} clearance. *A*: Averaged Ca^{2+} traces after a 300- or 400-ms step depolarization in control solution and CCCP (2 μmol/l) in cells not pretreated with TG. *B*: Averaged clearance in control solution or with CCCP (2 μmol/l) in TG-pretreated cells. These experiments were done with whole-cell voltage clamp in cells dialyzed with 5 mmol/l ATP.

of mitochondrial uptake by TG, since the same effect was seen with CPA-treated intact cells.

Relative contributions to Ca^{2+} clearance and a model. We now consider a more quantitative analysis. Clearance rates at each Ca^{2+} level were estimated from the measured slopes of the decay phase. Table 1 summarizes the relative contribution of each clearance mechanism as defined by use of inhibitors and calculated at four concentrations of $[Ca^{2+}]_i$. The SERCA pumps dominate. After SERCA pumps are inhibited, the NCX contributes relatively more to the clearance at high $[Ca^{2+}]_i$, whereas the PMCA contributes more at low $[Ca^{2+}]_i$. The sum of these three mechanisms accounts for 89–97% of the Ca^{2+} removal within the whole range of our tests.

Using these values, we developed a mathematical description of the three principal clearance mechanisms to simulate our experimental records (Fig. 2*B*, *D*, and *F*). We took conventional rate laws and values of coefficients from the literature for other cells where possible, and scaled the relative maximum fluxes to best correspond with our observations.

TABLE 1
Relative contribution of clearance systems to Ca^{2+} removal*

$[Ca^{2+}]_i$	0.5 μmol/l	0.9 μmol/l	1.5 μmol/l*	1.9 μmol/l
SERCA pumps	68	61	†	†
PMCA pumps	16	12	30†	35†
NCX	13	16	63†	62†
Total accounted for	97	89	93†	97†

Data are %. *The rate of $[Ca^{2+}]_i$ decay, $d[Ca^{2+}]_i/dt$, was determined at four $[Ca^{2+}]_i$ levels from averaged records. Table shows the percentage of the rate that was inhibited by appropriate blocking conditions. †Values from TG-pretreated cells, which represent the percentage contribution of the PMCA and NCX to the clearance (by the Na8.8 and Li7.4 methods) when SERCA pumps are disabled.

SERCA pumps were simulated by a saturating function with a Hill coefficient of 2.0:

$$M_{SERCA} = M_{\max SERCA} \times \frac{1}{1 + \left(\frac{K_{SERCA}}{[Ca^{2+}]_i}\right)^2} \quad (1)$$

where M is the Ca^{2+} flux. β-Cells express both the ubiquitous SERCA2b and the low-affinity SERCA3 pumps (13,14). For the half-saturating Ca^{2+} concentration (K_{SERCA}), we took a value for SERCA2b, 0.27 μmol/l (29). The PMCA was represented by simple Michaelis-Menten kinetics:

$$M_{PMCA} = M_{\max PMCA} \times \frac{1}{1 + \frac{K_{PMCA}}{[Ca^{2+}]_i}} \times \frac{[H^+]}{[H^+] + [K_a]} \quad (2)$$

with half-saturating concentration (K_{PMCA}) of 0.50 μmol/l (28) multiplied by a titration function expressing the activation of pumping by protons with a pKa of 7.86 (18). Bidirectional transport by the NCX is computed according to a complex rate equation derived from experiments on electrogenic transport in cardiac myocytes (28). For the NCX calculation, it was also necessary to model a time-varying intracellular concentration of Na^+, an obligate substrate of the exchanger. The model also had a small resting inward leak of Ca^{2+} from the bath through unspec-

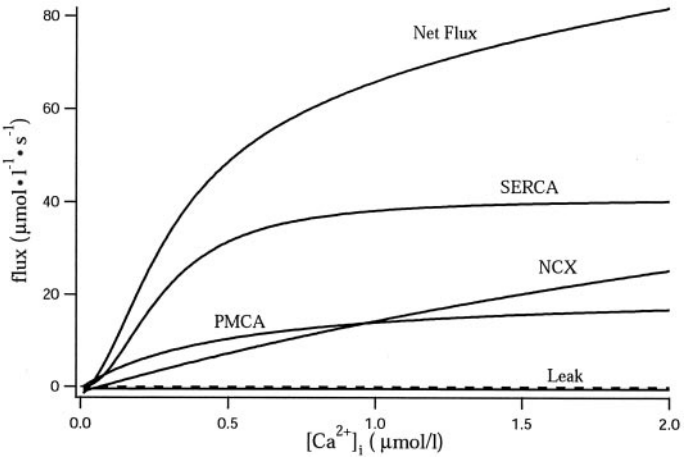

FIG. 6. Summary of the kinetic model for Ca^{2+} transport. Solutions of the rate equations for SERCA, NCX, PMCA, inward leak, and their sum (Net flux) under standard conditions are plotted against $[Ca^{2+}]_i$. The flux rates, in units of $\mu mol \cdot l^{-1} \cdot s^{-1}$, are >100-fold higher than the observed rates of change of $[Ca^{2+}]_i$ (Fig. 3*A*) because the model includes the effect of strong Ca^{2+} binding in the cytoplasm by endogenous buffers and by the indo-1 dye. Parameter values: the maximum efflux rates of SERCA and PMCA (at pH 7.4) pumps are 41 and 21 $\mu mol \cdot l^{-1} \cdot s^{-1}$ in the model; the velocity of the NCX at 1 μmol/l Ca^{2+} is 14 $\mu mol \cdot l^{-1} \cdot s^{-1}$; the steady rate of entry of Ca^{2+} via the resting leak is 0.47 $\mu mol \cdot l^{-1} \cdot s^{-1}$ with 2 mmol/l Ca^{2+} outside.

ified ion channels, and it assumed that the cytoplasm has an endogenous calcium binding ratio of 100:1 as well as additional Ca^{2+} buffering contributed by the indo-1 dye. We estimated the dye concentration in intact cells loaded by the indo-1-AM method by comparing the intensity of their fluorescence with the intensity of cells studied by whole-cell pipette with 100 μmol/l indo-1 in the pipette. By this method, the intact cells contained on average 188 μmol/l indo-1. This amount of dye raises the Ca^{2+} binding ratio from 100 to 178 when the free $[Ca^{2+}]_i$ is 500 nmol/l. The assumption of a Ca^{2+} binding ratio allows us to translate the observed rate of change of free $[Ca^{2+}]_i$ (units of moles per liter per second) into total calcium molar fluxes across the plasma or ER membranes of a liter of β-cells (units of moles per second). Errors in this assumption would scale the fluxes; i.e., if the total buffer is actually double that assumed, the fluxes would need to be doubled.

The relative flux rates of the model (Fig. 6 legend) were chosen so that the predicted time constants of clearance (Fig. 3*B*, ○) agreed with the experimental values (Fig. 3*B*, bars). The full Ca^{2+} time courses predicted from the model are shown in the righthand panels of Fig. 2. Comparison to the original data shows generally good agreement with the effects of various inhibitors. The simulated decay of $[Ca^{2+}]_i$ has an exponential time constant of 1.51 s for intact cells with 188 μmol/l indo-1, 1.43 s for whole-cell recording with 100 μmol/l indo-1 (and 10 Ca^{2+} outside), and 1.11 s for the physiological state when cells contain no dye (simulating a "physiological" state we could not measure experimentally). In the simulations of intact cells, KCl treatments were represented as 3-s depolarizations from –70 to –10 mV with a 350-fold enhanced Ca^{2+} influx rate. TG was assumed to turn off SERCA pumps fully. Inhibition of the PMCA was 86% at pH 8.8 (18), and only 62% by La^{3+} (assumed). Figure 6 summarizes the predicted clearance rates of each of the transport mechanisms as given by the model. The SERCA pumps account for about 60–70% of the clearance at all $[Ca^{2+}]_i$ levels and the PMCA and NCX account for the remainder.

SERCA pumps limit depolarization-induced secretion. Because inhibition of SERCA pumps significantly increased and prolonged depolarization-induced Ca^{2+} transients, we reasoned that it should also increase depolarization-induced exocytosis from the cell. Figure 7 shows $[Ca^{2+}]_i$ and amperometric recordings of exocytosis from β-cells during 10-s KCl depolarizations. Each current spike in the amperometric records indicates exocytosis of a single serotonin-containing secretory granule (see RESEARCH DESIGN AND METHODS). In a single cell (Fig. 7*B*) or a small cluster of cells (Fig. 7*C*), addition of CPA dramatically and reversibly raised the $[Ca^{2+}]_i$ level reached and increased the rate of exocytosis evoked by a long depolarization. On average, CPA increased exocytosis to 5.3 ± 1.0 times the control (n = 24).

DISCUSSION

Several observations reveal that SERCA pumps can remove cytoplasmic Ca^{2+} faster than the other transport mechanisms in dissociated pancreatic β-cells. Inhibitors of SERCA pumps increase the rate of rise and the size of depolarization-induced Ca^{2+} transients (3-s depolarizations), lengthen the time constant of decay, slow the rate of clearance, and increase the exocytotic response. The simplest approach to quantitation treats clearance as a first-order process, e.g., for clearance *time constants* of 1.7 s in intact calls (or 1.0 s in whole-cell clamp), the overall clearance *rate constant* would be 0.61 (or 1) s^{-1}. This would represent the sum of all clearance mechanisms acting in parallel. Addition of CPA or pretreatment with TG has similar effects on the two preparations; the time constants lengthen to 4.6 s (or 4.4 s). Thus, the rate constant of all non-SERCA clearance (mostly PMCA and NCX) is 0.22 (or 0.23) per second and that for SERCA clearance is 0.39 per s (or 0.77 per second with 5 mmol/l ATP in the pipette). In both cell preparations, the SERCA pump is faster than all others put together. The same result is seen in Fig. 6, which plots the modeled molar Ca^{2+} pumping rate for each of the three clearance mechanisms we found in intact cells. At all $[Ca^{2+}]_i$ concentrations >100 nmol/l, the SERCA pump is the fastest. Our results agree well with a previous report that TG prolongs the Ca^{2+} clearance time constant from 1.8 to 4.6 s in mouse β-cells and that Na^+-free solution has a much smaller effect, changing time constants from 2.0 to 2.6 s (30).

β-Cells cannot accomplish their physiological role using SERCA pumps alone. There is significant Ca^{2+} entry across the plasma membrane lasting many seconds during normal episodic insulin secretion. Although the SERCA pumps might continue to transport rapidly, efflux from the filling ER will soon counterbalance this clearance mechanism. In the long run, Ca^{2+} has to be pumped out of the cell rather than being accumulated in intracellular stores. Fortunately, there is an appreciable TG-insensitive component of clearance consisting at least of the PMCA and the NCX. Even in TG-pretreated cells exposed to Na^+-free solution that would stop the NCX, the $[Ca^{2+}]_i$ still returns fully to resting levels after a Ca^{2+} load. We confirm the observation of several groups (25,26) that following a

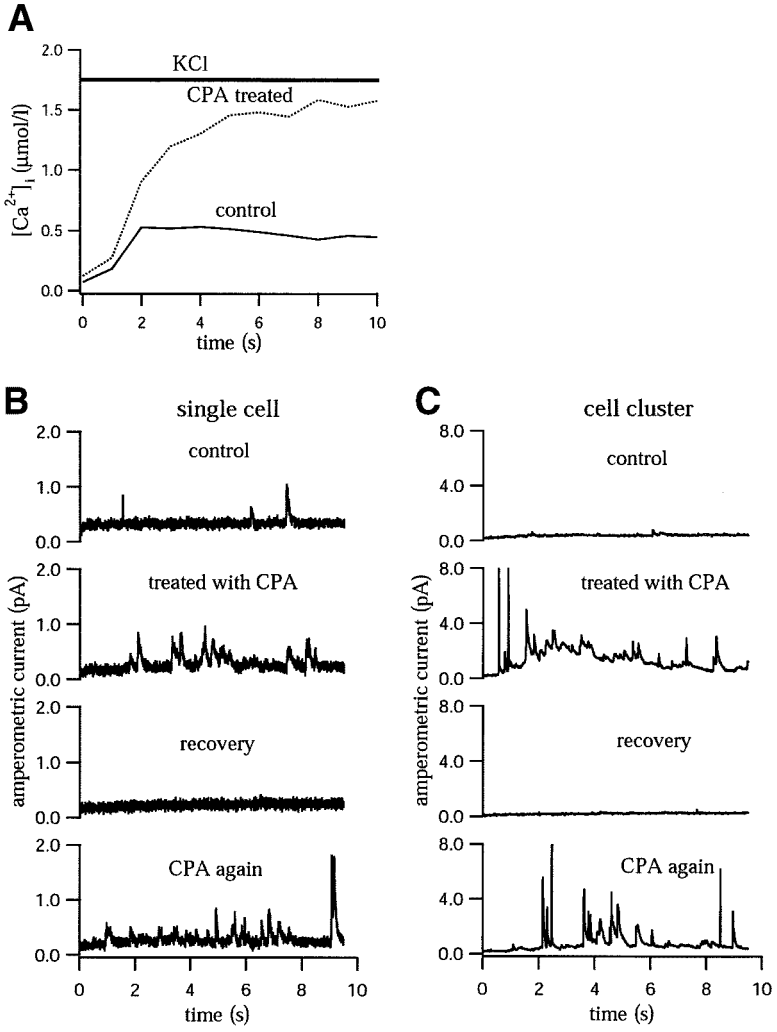

FIG. 7. SERCA pumps limit depolarization-triggered secretion. Time course of $[Ca^{2+}]_i$ (*A*) and time course of serotonin release detected by carbon-fiber amperometry during a 10-s depolarization in a serotonin-loaded single cell (*B*) or cell cluster (*C*). CPA (50 μmol/l) treatments increased the $[Ca^{2+}]_i$ transients and the frequency of the spikes.

round of Ca^{2+} clearance, the ER spontaneously returns a considerable amount of Ca^{2+} to the cytoplasm, lowering the ER content and prolonging the late phase of cytoplasmic clearance. This delayed release may reflect a combination of Ca^{2+}-induced Ca^{2+} release and rebalancing of the steady-state filling of the ER once $[Ca^{2+}]_i$ falls to low levels. It is potentially very significant during physiological secretion and deserves further quantitative investigation.

The relative contribution of the PMCA to Ca^{2+} clearance in β-cells has not been clearly established because of a lack of specific inhibitors. The criteria we used here have some drawbacks. High pH_o might change intracellular pH (and we have controlled for that), and it is known in other cells to enhance passive Ca^{2+} influxes in several voltage-gated Ca^{2+} channels by relieving proton block (31) and to depress the NCX (pH 10 depresses NCX by 51% [32]). Lanthanum has only a narrow window of usefulness as a specific agent since, at concentrations not quite sufficient to block the PMCA, it begins to block the NCX and to accumulate inside cells (19). Nevertheless, our results with the two methods are self-consistent with the overall partitioning of transport components obtained by use of these inhibitors and TG- and Na^+-free solutions. Several PMCA isoforms and several NCX isoforms are expressed in rat and human pancreatic β-cells and related cell lines (11,12,15).

Glucose and KCl can induce changes of mitochondrial membrane potential in pancreatic β-cells (33) and of mitochondrial Ca^{2+} concentration in a β-cell line (34). Hence, β-cell mitochondria, like those of other cells, transport Ca^{2+}. In the β-cell, however, we find that this transport rate is slower than that of the SERCA, PMCA, and NCX mechanisms, so by itself it does not contribute to the overall time course of clearance.

Another consideration is that emptying of ER stores by treatment with CPA or with inositol-trisphosphate-inducing agonists is reported to elicit store-operated inward calcium current in pancreatic β-cells (35,36). This could slow the apparent time course of clearance and lead to an underestimation of the clearance rates. In our TG-pretreated cells, the baseline $[Ca^{2+}]_i$ was only 12% higher than in untreated cells, so we suggest that any store-operated calcium current in our experiments is quite small relative to the other sources of Ca^{2+} leak and would not significantly alter our results.

In conclusion, our experiments and modeling provide a quantitative description of the Ca^{2+} clearance mechanisms of mouse pancreatic β-cells bathed in a saline solution with high glucose. Clearance is quite fast, and the initial phase is dominated by SERCA pumps. We demonstrate the significance of SERCA pumps in regulating excitation-secretion coupling. It is probable that several of

the transport mechanisms studied here could be altered by lowering the glucose concentration or by adding neurotransmitters to initiate intracellular signaling cascades. These conditions merit investigation. More work is also required to clarify the dynamic contributions of delayed Ca^{2+} release from the ER and to determine the endogenous Ca^{2+} binding ratio to calibrate the absolute flux rates of the transport mechanisms. These findings will be important to facilitate better understanding and prediction of insulin secretion.

ACKNOWLEDGMENTS

This work was supported by National Institutes of Health (NIH) Grant AR17803, by a Pilot and Feasibility Award from the University of Washington Diabetes Endocrinology Research Center (NIH Grant DK17047), and by KOSEF Grant R01-00285 (Korea).

The authors thank Fernando Santana, Donner Babcock, Lea Miller, and Jie Zheng for their helpful comments on the manuscript and Josep Vidal for advice with the β-cell preparation.

REFERENCES

1. Rutter GA: Nutrient-secretion coupling in the pancreatic islet β-cell: recent advances. *Mol Aspects Med* 22:247–284, 2001
2. Kasai H, Suzuki T, Liu TT, Kishimoto T, Takahashi N: Fast and cAMP-sensitive mode of Ca^{2+}-dependent exocytosis in pancreatic β-cells. *Diabetes* 51 (Suppl. 1):S19–S24, 2002
3. Ammala C, Eliasson L, Bokvist K, Berggren PO, Honkanen RE, Sjoholm A, Rorsman P: Activation of protein kinases and inhibition of protein phosphatases play a central role in the regulation of exocytosis in mouse pancreatic β cells. *Proc Natl Acad Sci U S A* 91:4343–4347, 1994
4. Renstrom E, Eliasson L, Rorsman P: Protein kinase A-dependent and -independent stimulation of exocytosis by cAMP in mouse pancreatic β-cells. *J Physiol* 502 (Pt 1):105–118, 1997
5. Eliasson L, Renstrom E, Ammala C, Berggren PO, Bertorello AM, Bokvist K, Chibalin A, Deeney JT, Flatt PR, Gabel J, Gromada J, Larsson O, Lindstrom P, Rhodes CJ, Rorsman P: PKC-dependent stimulation of exocytosis by sulfonylureas in pancreatic β cells. *Science* 271:813–815, 1996
6. Maechler P, Wollheim CB: Mitochondrial glutamate acts as a messenger in glucose-induced insulin exocytosis. *Nature* 402:685–689, 1999
7. Corkey BE, Glennon MC, Chen KS, Deeney JT, Matschinsky FM, Prentki M: A role for malonyl-CoA in glucose-stimulated insulin secretion from clonal pancreatic β-cells. *J Biol Chem* 264:21608–21612, 1989
8. Deeney JT, Gromada J, Hoy M, Olsen HL, Rhodes CJ, Prentki M, Berggren PO, Corkey BE: Acute stimulation with long chain acyl-CoA enhances exocytosis in insulin-secreting cells (HIT T-15 and NMRI β-cells). *J Biol Chem* 275:9363–9368, 2000
9. Aspinwall CA, Lakey JR, Kennedy RT: Insulin-stimulated insulin secretion in single pancreatic β cells. *J Biol Chem* 274:6360–6365, 1999
10. Aspinwall CA, Qian WJ, Roper MG, Kulkarni RN, Kahn CR, Kennedy RT: Roles of insulin receptor substrate-1, phosphatidylinositol 3-kinase, and release of intracellular Ca^{2+} stores in insulin-stimulated insulin secretion in β-cells. *J Biol Chem* 275:22331–22338, 2000
11. Kamagate A, Herchuelz A, Bollen A, Van Eylen F: Expression of multiple plasma membrane Ca^{2+}-ATPases in rat pancreatic islet cells. *Cell Calcium* 27:231–246, 2000
12. Van Eylen F, Svoboda M, Herchuelz A: Identification, expression pattern and potential activity of Na/Ca exchanger isoforms in rat pancreatic β-cells. *Cell Calcium* 21:185–193, 1997
13. Varadi A, Molnar E, Ashcroft SJ: Characterisation of endoplasmic reticulum and plasma membrane Ca^{2+}-ATPases in pancreatic β-cells and in islets of Langerhans. *Biochim Biophys Acta* 1236:119–127, 1995
14. Varadi A, Molnar E, Ostenson CG, Ashcroft SJ: Isoforms of endoplasmic reticulum Ca^{2+}-ATPase are differentially expressed in normal and diabetic islets of Langerhans. *Biochem J* 319 (Pt 2):521–527, 1996
15. Varadi A, Molnar E, Ashcroft SJ: A unique combination of plasma membrane Ca^{2+}-ATPase isoforms is expressed in islets of Langerhans and pancreatic β-cell lines. *Biochem J* 314 (Pt 2):663–669, 1996
16. Lernmark A: The preparation of, and studies on, free cell suspensions from mouse pancreatic islets. *Diabetologia* 10:431–438, 1974
17. Rorsman P, Trube G: Calcium and delayed potassium currents in mouse pancreatic β-cells under voltage-clamp conditions. *J Physiol* 374:531–550, 1986
18. Xu W, Wilson BJ, Huang L, Parkinson EL, Hill BJ, Milanick MA: Probing the extracellular release site of the plasma membrane calcium pump. *Am J Physiol Cell Physiol* 278:C965–C972, 2000
19. Shimizu H, Borin ML, Blaustein MP: Use of La^{3+} to distinguish activity of the plasmalemmal Ca^{2+} pump from Na^+/Ca^{2+} exchange in arterial myocytes. *Cell Calcium* 21:31–41, 1997
20. Herrington J, Park YB, Babcock DF, Hille B: Dominant role of mitochondria in clearance of large Ca^{2+} loads from rat adrenal chromaffin cells. *Neuron* 16:219–228, 1996
21. Grynkiewicz G, Poenie M, Tsien RY: A new generation of Ca^{2+} indicators with greatly improved fluorescence properties. *J Biol Chem* 260:3440–3450, 1985
22. Best L, Elliott AC: Changes in 2′,7′-bis(carboxyethyl) 5′(6′)-carboxyfluorescein-, fura-2 and autofluorescence in intact rat pancreatic islets in response to nutrients and non-nutrients. *Mol Cell Endocrinol* 111:191–198, 1995
23. Smith PA, Duchen MR, Ashcroft FM: A fluorimetric and amperometric study of calcium and secretion in isolated mouse pancreatic β-cells. *Pflugers Arch* 430:808–818, 1995
24. Koh DS, Hille B: Rapid fabrication of plastic-insulated carbon-fiber electrodes for micro-amperometry. *J Neurosci Methods* 88:83–91, 1999
25. Gilon P, Arredouani A, Gailly P, Gromada J, Henquin JC: Uptake and release of Ca^{2+} by the endoplasmic reticulum contribute to the oscillations of the cytosolic Ca^{2+} concentration triggered by Ca^{2+} influx in the electrically excitable pancreatic β-cell. *J Biol Chem* 274:20197–20205, 1999
26. Lemmens R, Larsson O, Berggren PO, Islam MS: Ca^{2+}-induced Ca^{2+} release from the endoplasmic reticulum amplifies the Ca^{2+} signal mediated by activation of voltage-gated L-type Ca^{2+} channels in pancreatic β-cells. *J Biol Chem* 276:9971–9977, 2001
27. Hopkins WF, Satin LS, Cook DL: Inactivation kinetics and pharmacology distinguish two calcium currents in mouse pancreatic β-cells. *J Membr Biol* 119:229–239, 1991
28. Weber CR, Ginsburg KS, Philipson KD, Shannon TR, Bers DM: Allosteric regulation of Na/Ca exchange current by cytosolic Ca in intact cardiac myocytes. *J Gen Physiol* 117:119–131, 2001
29. Lytton J, Westlin M, Burk SE, Shull GE, MacLennan DH: Functional comparisons between isoforms of the sarcoplasmic or endoplasmic reticulum family of calcium pumps. *J Biol Chem* 267:14483–14489, 1992
30. Gall D, Gromada J, Susa I, Rorsman P, Herchuelz A, Bokvist K: Significance of Na/Ca exchange for Ca^{2+} buffering and electrical activity in mouse pancreatic β-cells. *Biophys J* 76:2018–2028, 1999
31. Prod'hom B, Pietrobon D, Hess P: Direct measurement of proton transfer rates to a group controlling the dihydropyridine-sensitive Ca^{2+} channel. *Nature* 329:243–246, 1987
32. Egger M, Niggli E: Paradoxical block of the Na^+-Ca^{2+} exchanger by extracellular protons in guinea-pig ventricular myocytes. *J Physiol* 523 (Pt 2):353–366, 2000
33. Kindmark H, Kohler M, Brown G, Branstrom R, Larsson O, Berggren PO: Glucose-induced oscillations in cytoplasmic free Ca^{2+} concentration precede oscillations in mitochondrial membrane potential in the pancreatic β-cell. *J Biol Chem* 276:34530–34536, 2001
34. Kennedy ED, Rizzuto R, Theler JM, Pralong WF, Bastianutto C, Pozzan T, Wollheim CB: Glucose-stimulated insulin secretion correlates with changes in mitochondrial and cytosolic Ca^{2+} in aequorin-expressing INS-1 cells. *J Clin Invest* 98:2524–2538, 1996
35. Dyachok O, Gylfe E: Store-operated influx of Ca^{2+} in pancreatic β-cells exhibits graded dependence on the filling of the endoplasmic reticulum. *J Cell Sci* 114:2179–2186, 2001
36. Liu YJ, Gylfe E: Store-operated Ca^{2+} entry in insulin-releasing pancreatic β-cells. *Cell Calcium* 22:277–286, 1997